

Venus Monitoring Camera for Venus Express

W.J. Markiewicz¹, D. Titov^{1,4}, B. Fiethe², T. Behnke³, I. Szemerey¹, H. Perplies¹, M. Wedemeier¹, I. Sebastian¹, W. Boogaerts¹, C. Dierker², D. Osterloh², N. Ignatiev⁴, M. Koch², H.U. Keller¹, R. Jaumann³, H. Michaelis³, H. Michalik², D. Crisp⁵, L. Esposito⁶, S.S. Limaye⁷, S. Watanabe⁸, N. Thomas⁹, D. Belyaev⁴, A. Dannenberg¹, M. Tchimel¹, R. Moissl¹

¹*Max-Planck-Institute for Solar System Research, Max-Planck-Str. 2, 37191 Katlenburg-Lindau, Germany*

email markiewicz@mps.mpg.de

²*IDA Technical University Braunschweig, Germany*

³*German Aerospace Center (DLR), Berlin, Germany*

⁴*Space Research Institute (IKI), Moscow, Russia*

⁵*Jet Propulsion Laboratory, Pasadena, CA, USA*

⁶*Laboratory for Atmospheric and Space Physics, Boulder, CO, USA*

⁷*University of Wisconsin, Madison, WI, USA*

⁸*Hokkaido University Sapporo, Japan*

⁹*University of Bern, Switzerland*

The Venus Monitoring Camera (VMC) is part of the Venus Express payload. One of the main goals of the Venus Express mission is to study the dynamics of the Venus atmosphere. This objective requires global imaging of the planet. The VMC is designed to meet this goal having a relatively wide field of view of 17.5°. The VMC will take images of Venus in four narrow band filters from UV to near-IR all sharing one CCD. The spatial resolution will be 0.2 km to 45 km per pixel, depending on the distance from the planet. The full disc of Venus will be in the VMC FOV near the apocentre of the orbit. The VMC will complement other instruments of Venus Express by, 1) tracking cloud motions at ~70 km (cloud tops) and at ~50 km (main cloud layer) altitude; 2) mapping O₂ night-glow and its variability 3) mapping the night side thermal emission from the surface and studying of the lapse rate and H₂O content in the lower 6-10 km. In addition the VMC will provide imaging context for the whole mission and its movies of Venus atmosphere will be of significant interest for science as well as for the public outreach programme.

Introduction

The Venus Express mission will focus on the global investigation of the Venus atmosphere and plasma environment. It will also address some important aspects of geology and surface physics. The originally proposed core payload of this mission was composed of instruments available from the Mars Express and Rosetta projects. They were SPICAM, PFS, ASPERA, VIRTIS and VeRa. Further details about the mission and these instruments can be found in accompanying articles in this volume. This core payload, although capable of performing great science at Venus was missing a wide angle imaging instrument. The only imaging instrument (VIRTIS) has a field of view of $\sim 4^\circ$ that is far too narrow to routinely observe the global pattern of atmospheric motions. Complete coverage of the planet's disc by this experiment requires complex spacecraft re-pointing which will only be possible occasionally from the apocentre of the orbit. At the same time the study of global dynamics is one of the main goals of the Venus Express mission. It is for these reasons that we proposed to build a relatively simple wide angle camera with narrow band filters focusing on a few specific science goals. In this way the Venus Monitoring Camera (VMC) project was started. The present paper describes VMC, its science goals, some of the key calibration data as well as planned modes of the operations at Venus. The original VMC design foresaw six optical filters and two CCD detectors. The VMC, although having partial heritage from Rosetta and Mars Express missions, is a new development. The limited time and resources forced us to compromise to having only four channels and one CCD.

Scientific objectives

The VMC instrument using dedicated narrow angle filters and CCD detector with a sensitivity range from 0.3 to 1.0 μm will achieve the scientific goals described below. The main focus of this experiment will be to observe the dynamical phenomena in the Venus atmosphere in the altitude range from thermosphere (~ 150 km) to the main cloud deck (~ 50 km), as well as sounding of the surface through the 1 micron window.

Daytime observations in the UV-blue spectral range

The spectrum of solar radiation reflected by Venus has broad absorption feature between 0.2 and 0.5 μm (Fig. 1) (Moroz, 1985). The region between 0.2 and 0.32 μm is well explained by the presence of SO_2 at the cloud tops. The spectrum above 0.32 μm implies the presence of another absorber that has not been identified so far. Identifying it is important because due to this species Venus absorbs about 50% of solar radiation at the cloud top level. This has implications for the energy balance and dynamics of the whole atmosphere. Inhomogeneity in spatial and/or vertical distribution of the unknown absorber produces the famous UV features on the Venusian's disc (Figure 2). Tracking their motions has been usually used to study the dynamics of the cloud tops, i.e. to measure the winds and observe the wave phenomena. The typical size of most of the UV features does not exceed 100 km. One exception is the global Y feature. Their motions mark the super-rotation of the Venus cloud tops at ~ 67 km altitude with zonal velocity of about 100 m/s and ten times slower meridional speed. With this objectives in mind one of the VMC filters was chosen to cover the spectral range from 345 to 385 nm. It will be used to study,

- *the spatial and vertical distribution of the UV-blue absorbers at the cloud tops;*
- *the dynamics of cloud tops by tracing the motions of UV features;*
- *the vertical distribution of haze above the main cloud layer.*

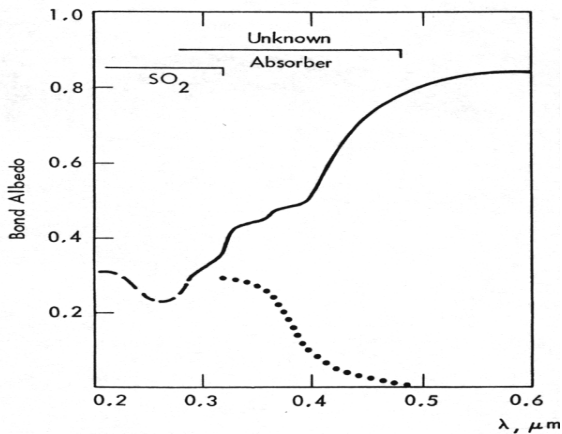


Figure 1 UV-visible spectrum of Venus' spherical albedo (solid) and contrast (dots).



Figure 2 Mariner 10 image of Venus.

Observation of the visible airglow at the nightside

Several types of airglow were observed on the Venus nightside. The spectrometer experiment onboard Venera-9 and -10 discovered strong airglow in the visible (Krasnopolsky, 1983). Figure 3 shows the airglow spectrum that led to the unambiguous identification of the Herzberg I and II systems of O₂ with a total intensity of ~3 kR. Limb observations showed that this emission originates in a layer at 90-110 km altitude.

The second VMC filter is positioned roughly in the middle of the Herzberg system with the spectral range from 503 to 523 nm. Mapping the airglow spatial distribution and its temporal variations with this filter will contribute to the study of the circulation of the lower thermosphere (100-130 km). Limb imaging will be used to study the high altitude haze layers. In addition these observations will also continue the search for lightning and measure the visible albedo of Venus.

Surface and lower atmosphere emission in the 1 μm transparency “window”

The discovery of spectral “windows” in the near IR spectrum of Venus (Allen and Crawford, 1984), through which thermal radiation from the hot lower atmosphere and even surface can leak

to space, provide a powerful tool to study the atmosphere below the clouds. These weak emissions can be observed only on the night side of the planet. Figure 4 shows a synthetic spectrum of the Venus nightside (Ignatiev, private communication) together with that measured by the VIMS instrument during the Cassini fly-by (Baines et al., 2000). Ground based observations (Figure 4), and subsequent radiative transfer modeling show that the 1 μm “window” emission originates at the surface (Meadows and Crisp, 1996). The thick atmosphere and cloud layer contribute only to conservative scattering of the radiation but not to emission.



Figure 3 Ground-based observations of the Venus nightside in 1 micron transparency “window”.

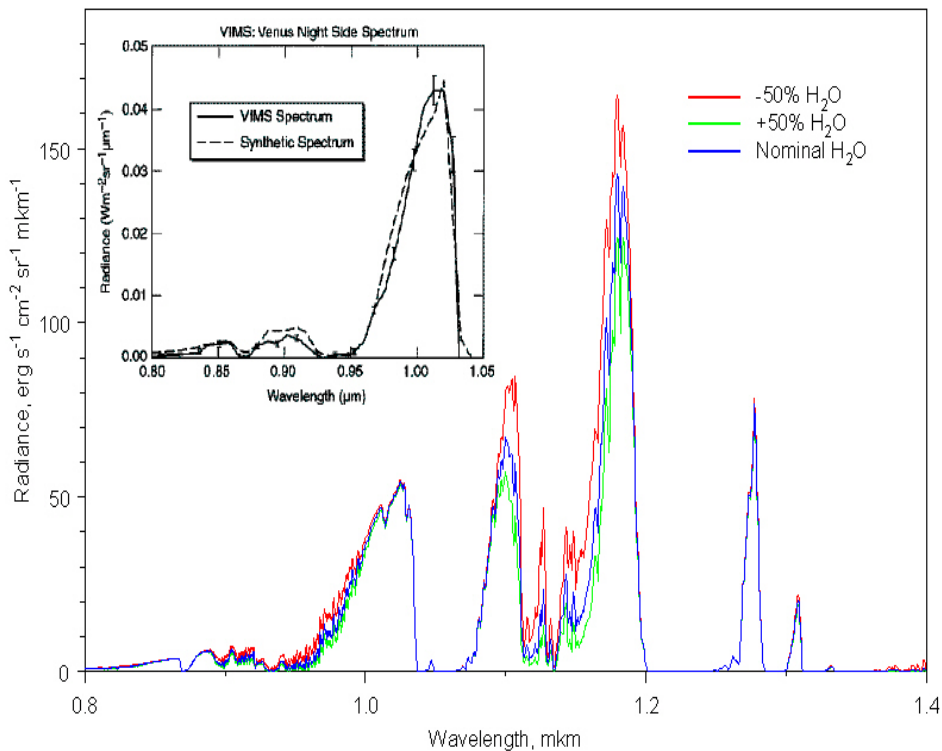


Figure 4 Synthetic spectrum of the radiation from the Venus nightside and Cassini/VIMS measurements of the 1 μm emission.

Imaging the Venus nightside at 1 μm would yield the spatial distribution of the surface brightness temperature attenuated by diffuse scattering in the atmosphere and cloud layer. Figure 5 shows the ground-based images of Venus obtained in several different “windows” near 1 μm (Meadows and Crisp, 1996). At 1.31, 1.28, and 1.18 μm the atmospheric emission prevails and the brightness pattern is due to inhomogeneities of the cloud opacity. Tracking the motions of these features would characterize the wind speeds at ~ 50 km altitude. At shorter wavelengths (1.1, 1.0 μm) the surface emission becomes dominant and brightness distribution correlates with topography: the higher the region the darker it appears on the image. This adds the pattern of surface origin to that defined by the clouds (Figure 3). Thus a sequence of such images taken

from orbit can provide information on both the surface and cloud layer. Moreover, Meadows and Crisp (1996) showed that the mapping in 1 μm window could be effectively used to derive the lapse rate in the lower 6 km.

Figure 4 shows that the short-wavelength side of the 1 μm emission peak is sensitive to the water vapour abundance in the lower atmosphere. Thus mapping the emission at $\sim 0.97 \mu\text{m}$ in addition to 1 μm could yield the global distribution of the water vapour in the lower scale height.

The VMC has two NIR filters with spectral ranges 900-970 and 990-1030 nm. They will be used together to accomplish the following scientific goals.

- *Mapping the surface brightness temperature distribution*
- *Determination of the H₂O global distribution in the lower 10 km*
- *Determination of the lapse rate in the lower 6-8 km of the atmosphere*
- *Search for “hot spots” associated with volcanic activity*
- *Monitoring the atmospheric column opacity and its variations*
- *Study of the circulation of the main cloud deck*

The first four of these observations will be done with data from the nightside. For the circulation of the main cloud deck, data from both night and dayside will be useful.

The VMC Instrument

Overview and accommodation

The VMC consists of one unit that houses the optics, CCD and readout electronics (CRE), digital processing unit (DPU), and the power converter (POC). A Peltier element connected to the bottom of the CCD will cool the detector. In order to avoid moving parts (filter wheel) the camera is designed so that four objectives (channels) share a single CCD. The stray light protection is provided by external and internal baffles. The VMC is mounted on the +Y wall inside the spacecraft (Fig 7). A summary of the performance characteristics of the VMC components is given in the Table 1. The image data from CCD are read out by CRE and sent to the 1 Gbit mass memory integrated within the DPU. This DPU is a so-called "system-on-a-chip" (SoC) approach, which integrates all DPU functions into a single chip and therefore results in a miniaturised implementation. The processor is based on a “LEON-2” SPARC V8 compatible core, implemented in a radiation hardened Xilinx Virtex FPGA. Before image data is sent to spacecraft via high speed IEEE 1355 interface, different image processing functions (e.g. flat-fielding or JPEG2000 compression) can be done real time or offline. All VMC internal functions can be configured by the build-in “On-board Command Language” OCL, which allows the execution of user definable scripts in parallel working virtual machines.

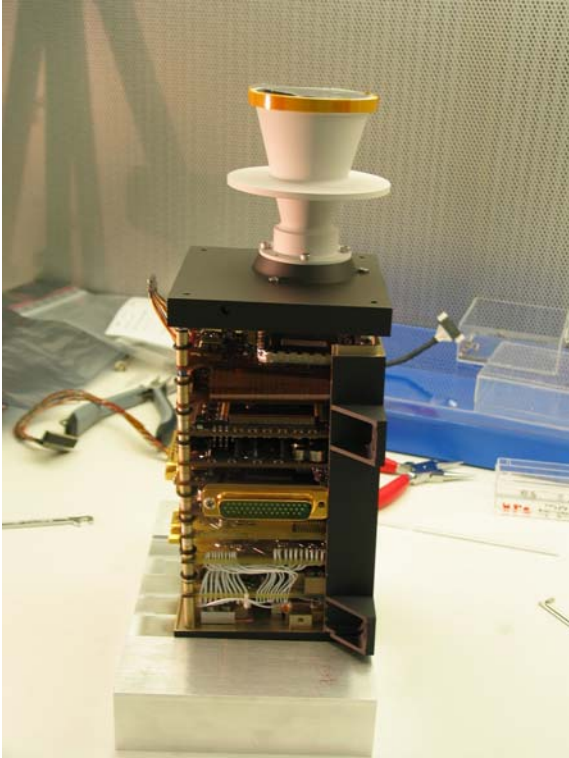


Figure 5 The VMC with one side of the housing removed, showing the CCD, DPU and power converter boards (top to bottom).

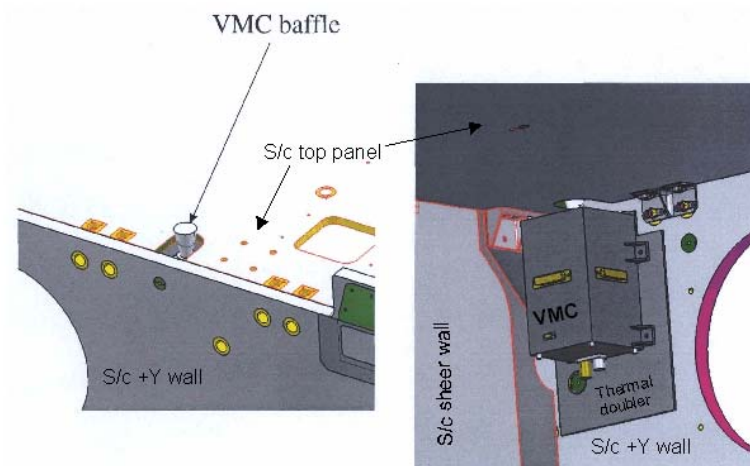


Figure 6 Accommodation of VMC on the spacecraft.

Table 1. Main performance parameters of the VMC instrument

Item	Specification
Optics	
General concept	Four objectives sharing a single CCD
Total field of view	~ 17.5° (0.3 rad)
Image scale	~ 0.74 mrad/px
Detector and CCD readout electronics (CRE)	
Type	Kodak KAI-1010, front illuminated, interline architecture, antiblooming
Detector size	1032(H)x1024(V)
Pixel size	9.0x9.0 μm
Full well	30,000 electrons
Total noise	~ 100 e @ +37 C
Dark current	~ 3000*2**(-(40-t,C)/8), e/s/px
Readout frequency	2.08896 MHz
Integration time	N*0.504 ms, N=1,2,3...64449
Power consumption	2.0W secondary
Operational temperature range	-30°C to +50°C
Non-ops temperature range	-50°C to 70°C
DPU	
Processor	<ul style="list-style-type: none"> • LEON-2 core (SPARC compatible) • 20 MIPS
Memory	<ul style="list-style-type: none"> • 1 Gbit image mass storage (SDRAM) • 16 Mbit SRAM • 16 Mbit EEPROM (Program memory) • 64 kbit PROM (Bootloader)
Power consumption	3.2W secondary
Power Converter (POC)	
Converter	4 Delta/VPT RT Converter
Power consumption	Efficiency η = 0.5..0.75

Optical Design

The VMC has four independent optical channels sharing one CCD. The optical design is presented in the Table 2. The VMC optics have been manufactured by FISBA OPTIK, St. Gallen, Switzerland. The figures 7 to 9 show pictures of VMC optics and of VMC camera.

Table 2. Optical design of VMC

VMC Channel	VIS	NIR1	NIR2	UV
Spectral range	503 – 523 nm	900 – 970 nm	990 – 1030 nm	345 – 385 nm
Center wavelength	513 nm	935 nm	1.01 μm	365 nm
Focal length	13 mm	13 mm	13 mm	13 mm
F-Number	5	5	5	7
Optics	3 Identical Cooke Triplets + curved front filter			Separate Cooke Triplet + curved front filter
Stop	Central obscuration			No obscuration
CCD	Kodak KAI-1010 Series, 1024 x 1024 pixel interline CCD, 9 μm pixel pitch			
Used area for	1. quadrant of	2. Quadrant of	3. Quadrant of	4.

imaging	CCD	CCD	CCD	Quadrant of CCD
Optical Layout				



Figure 7 Rear View of VMC Optics (green: VIS, purple: NIR channels)

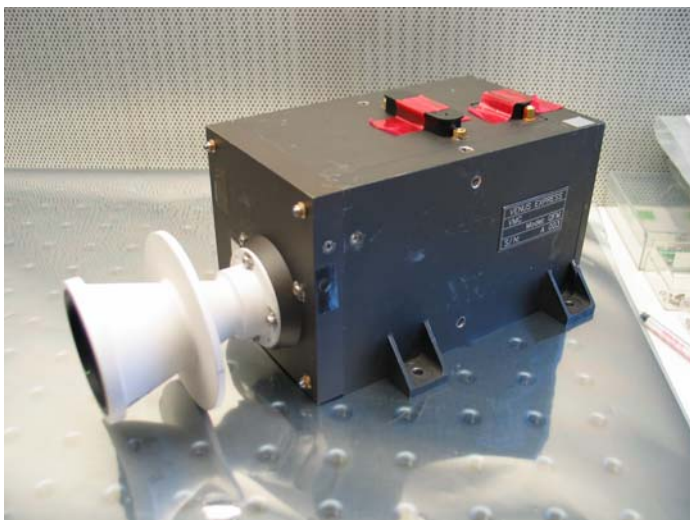


Figure 8 VMC Side View (QFM)

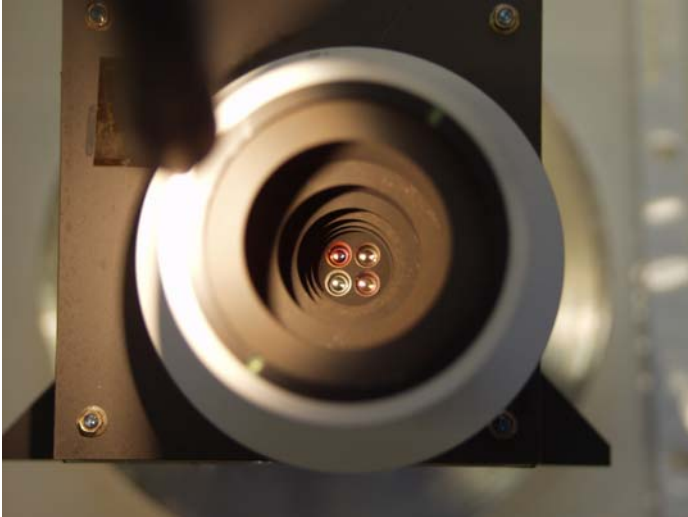


Figure 9 VMC Front View (QFM)

Obscuration spot for reducing ghost images

“Ghost image” inside of a CCD camera results from multiple reflections between the CCD surface and the surfaces of the lenses. The reflected light returns to the CCD and produces a secondary, or “ghost image”, in a different position on the CCD than the primary image. Although this secondary image is normally much weaker than the primary, for the application of observing the night side of Venus it is of crucial importance. The point is that the night side emission is so weak that it is completely dominated by the ghost of the dayside crescent. To suppress the ghost image we have glued an absorbing light trapping disk in the stop of the optics. The results of a ray tracing calculation with such an obscuration spot is shown in Fig. 11. The spot can also be seen in the VIS channel in Fig. 8. This type of ghost suppression was implemented in the VIS and in both NIR optics of the VMC. Ghosts are completely suppressed and could not be seen in the VMC calibration images.

Science Observations in Orbit

In flight the VMC will have several operation modes to cover all possible observation goals and conditions. The modes are: *pericentre*, *transmission*, *monitoring*, and *limb*. Table 3 summarizes main parameters of the VMC modes.

Pericenter mode

The *pericenter* mode will be used to study small scale dynamics and the fine cloud structure with high spatial resolution. It will be used when the spacecraft is within 250-10,000 km from the planet (Fig. 12). At such short distance VMC will be the only imaging instrument. Figure 12 shows a sketch of VMC fields of view covering the Northern hemisphere of Venus. The images collected during a pericentre pass will be stored in the VMC internal memory and send to the spacecraft afterwards in *transmission* mode.

Monitoring mode

The *monitoring* mode will be used to study the global atmospheric dynamics from distance for relatively long time: ~8 hours in ascending arc of the orbit or ~2 hours in the vicinity of pericentre. In figure 2.3.2 hatched area shows the size of the VMC field of view relative to the Venus disc represented by a yellow circle.

Limb sounding mode

In the *Limb* mode, VMC will study vertical structure of atmospheric hazes above the clouds.

Table 3. VMC Modes and their parameters

	Pericenter	Monitoring	Limb
Distance	250 – 10,000 km	10,000 – 66,000 km	~ 2,000 km
Total FOV	70 – 3,000 km	3,000 – 20,000 km	~ 500 km
Spatial Resolution	0.2 – 7 km	7 – 45 km	~ 1.5 km
Time between Images	5 – 300 s	~ 10 min	~ 10 s

Calibration and Performance

This section contains brief description of the VMC properties and behavior that had been investigated during the on-ground instrument characterization. Results of radiometric calibration are missing as the analysis of these data is still not completed.

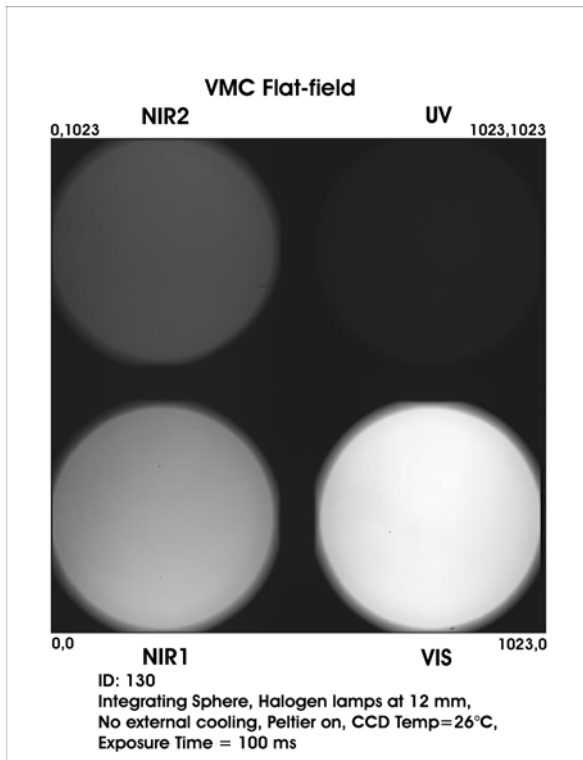


Figure 10 VMC flat field showing the four channels on one CCD

CCD Performance

To verify the electro-optical performance of the detector including readout electronics the photon-transfer-technique is used to specify total noise in darkness and system gain. At different exposure times images are acquired with and without light. Illumination is performed with light from a diffuse shined radiator based on red LEDs. The exposure is controlled via the EGSE PC (on/off of the LEDs). The linearity error of VMC CCD is in the range less than 1%. Figure 14 shows the quantum efficiency of the VMC CCD. To separate the noise performance of the

detector from the readout electronics also the CRE electronics was TV tested without CCD. In this configuration the CRE electronics input was grounded (no CCD). The noise of the readout electronics is in the range of 5 electrons at 2 MHz pixel frequency. As expected the exposure time control has no influence. Figure 15 shows a test images taken with the VMC CCD.

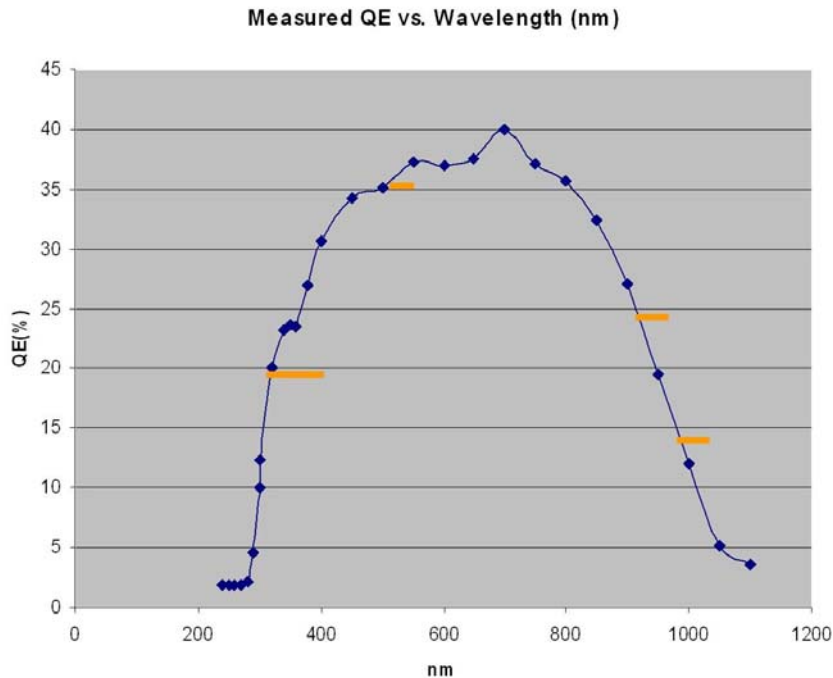


Figure 11 The VMC CCD Quantum Efficiency (measured)

Focus Measurements

The best focus curve for final adjustment prior to environmental tests (purple) is shown in figure 16. This focus check within VIS channel on-axis was performed several times between environmental tests in order to confirm that vibrations or TV tests had not distorted the focus. Full focus test for all 4 channels was performed during laboratory calibration at three temperatures: room, +40C, and -20C. In all cases defocusing was not detectable or was low and within the range of depth of field of $\pm 25 \mu\text{m}$. Hot temperature case with camera temperature of +36C and CCD temperature of +48C results in just acceptable camera defocus of + 30 μm .

Dark Signal Properties

Dark Signal Behavior with Temperature and Exposure

The VMC dark signal is a sum of dark current that is a function of temperature and exposure time and a bias, a constant electronics offset which is about 3300-3400 DNs. Figure 17 shows the dependence of the dark signal with temperature and exposure time. For temperatures below $\sim 35\text{C}$ and all available exposures (0.5ms-30s) the dark signal is defined by the bias. At temperatures above 40C the increase of dark current with temperature becomes dominant.

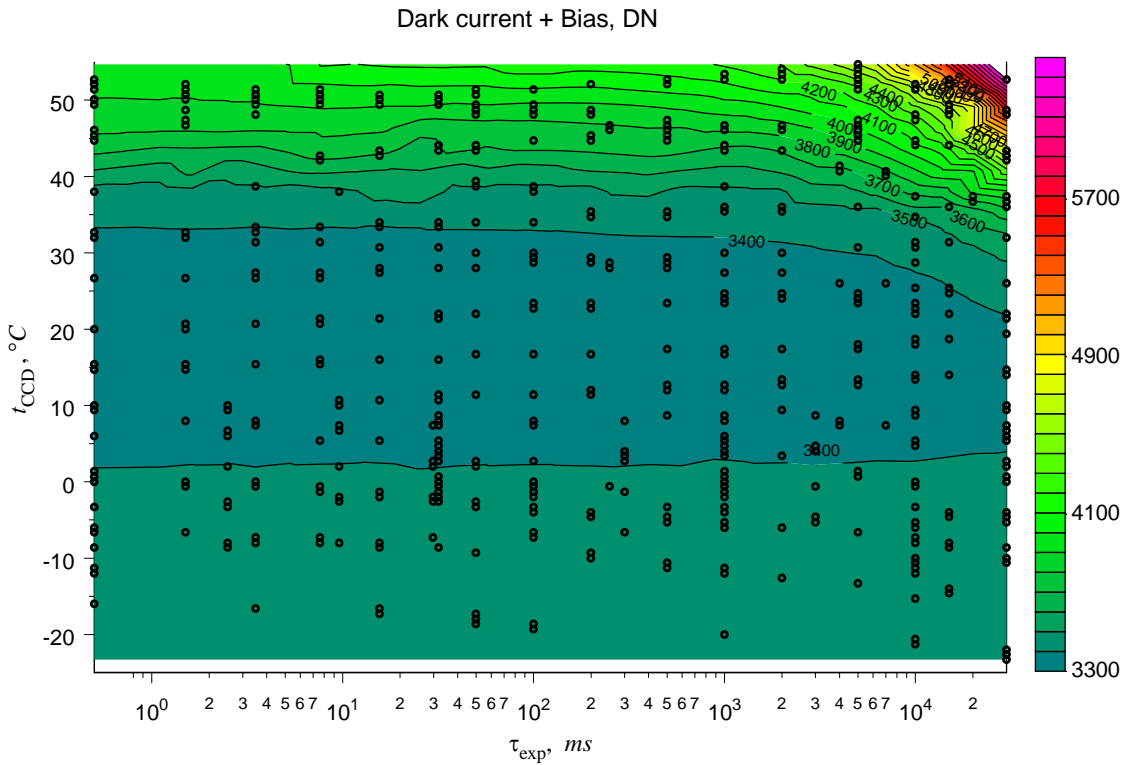


Figure 12 Dark signal as a function of the exposure time and CCD temperature, average over whole matrix except hot pixels and shaded boundary frame. Measured points are shown with the black circles

Dark Signal Noise

Figure 18 shows the field of dark signal noise as a function of exposure time and the CCD temperature. This plot represents standard deviation of the CCD counts obtained by subtraction of two images taken one after another using the same exposure time. Except for the region of high temperatures and high exposures the dark noise is below 25 DN which is close to the standalone CCD noise. Note that the standard deviation of the dark signal in each single image is much higher which indicates that each CCD pixel behaves individually and that a matrix of dark current noise instead of a single value should be used for dark current correction.

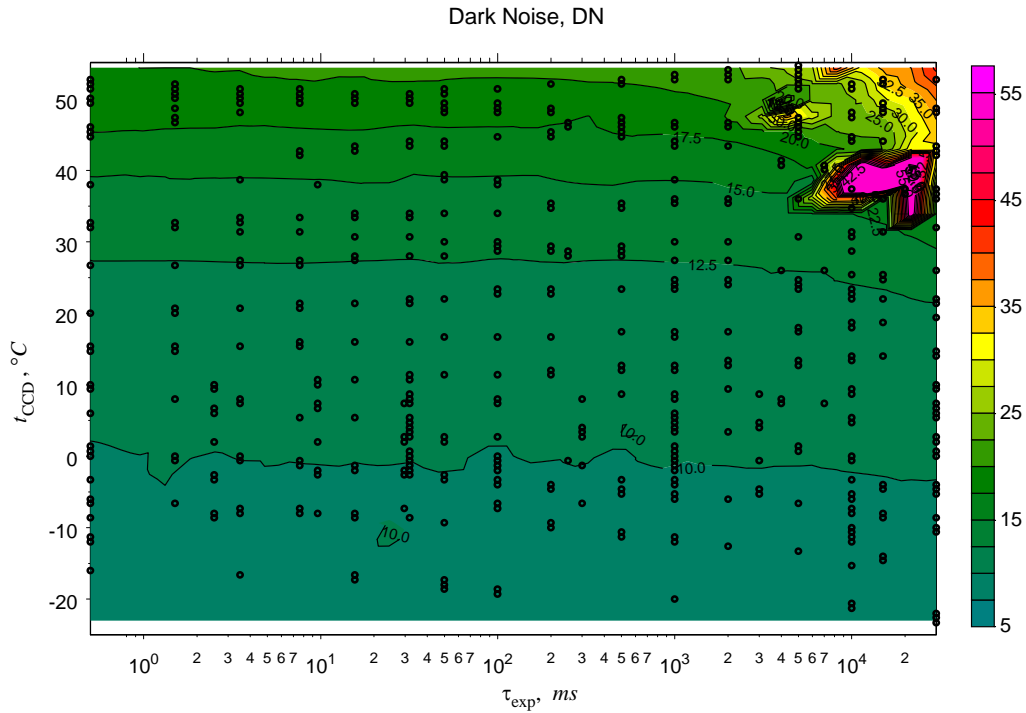


Figure 13 Dark signal noise as a function of the exposure time and CCD temperature, average over whole matrix except hot pixels and shaded boundary frame. Measured points are shown with the black circles

Spectral Properties

Spectral properties of four channels were determined in the laboratory calibrations. Figures 19 and 20 show comparison of the measured spectral properties with those specified in original VMC optics specification.

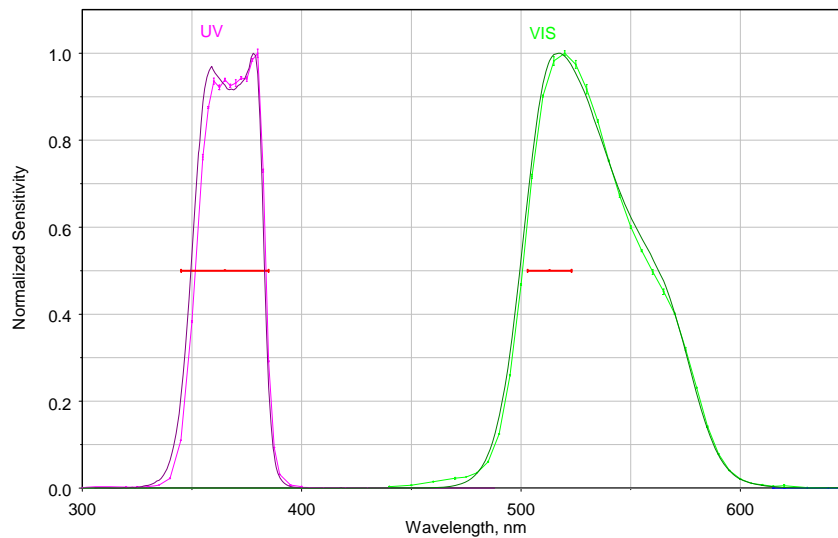


Figure 14 Normalized spectral sensitivities of the VMC UV and VIS channels. Bright curves with error bars: measurements at MPS; dark curves: sensitivities derived from the CCD quantum efficiency and filter transmissions provided by manufacturers; red bars: original specification

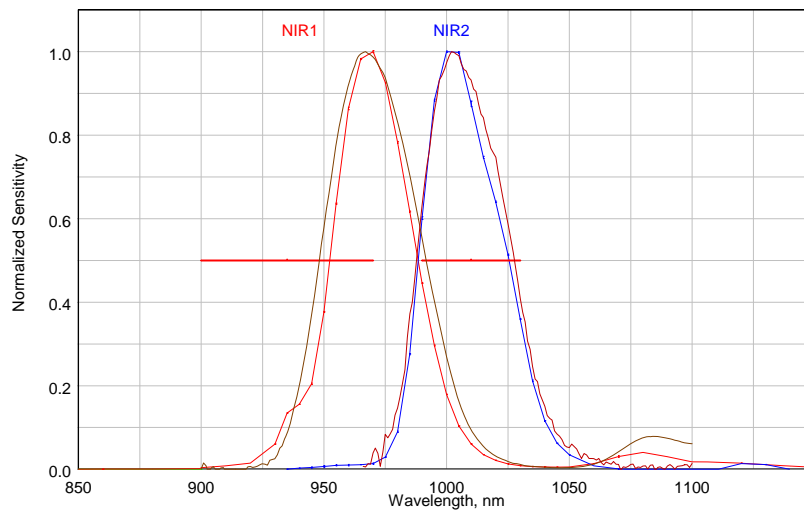


Figure 15 The same as figure 19 but for the NIR channels

Expected in-flight performance

Simulation of in-flight operations during the VMC FS TV tests together with numerical modeling of the spacecraft thermal behaviour in typical orbital cases carried out by Astrium (CDR study) allows one to predict CCD temperatures expected in flight. Figure 21 shows the dark signal as function of CCD temperature and exposure time (colored curves) as measured during VMC FS calibration. Red horizontal bars show ranges of CCD temperatures expected in flight for typical VEX observations (science cases) as follows from the Astrium thermal modeling and VMC FS performance during the TV tests. Important conclusion is that for all planned observations the CCD temperature falls in the optimal domain in which dark signal and dark noise are close to their minimal values and have weak dependence on CCD temperature and exposure time.

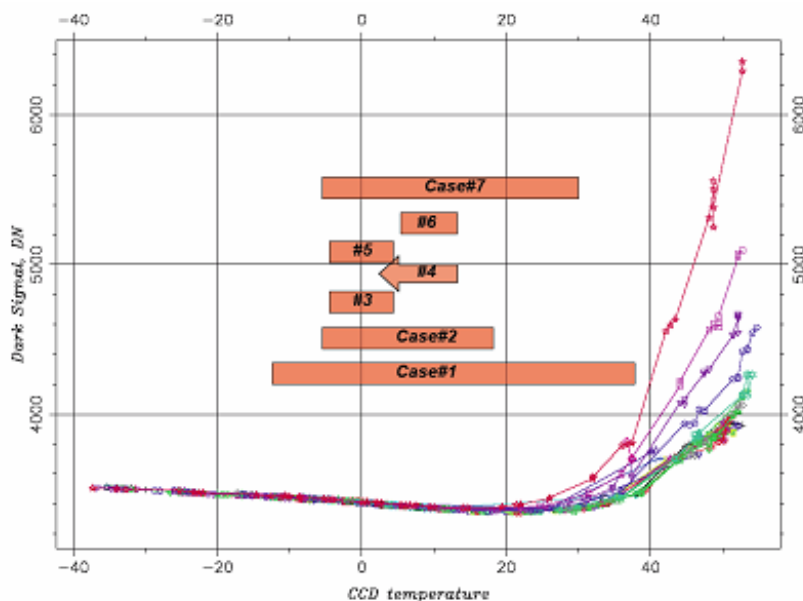


Figure 16 Dependence of the VMC dark signal on the CCD temperature at different exposures (colored curves). Red horizontal bars show temperature ranges expected in flight in different science cases as follows from the Astrium thermal analysis (CDR study)

References

Allen, D. and J.W. Crawford, Cloud structure on the dark side of Venus, *Nature* 307, 222-224, 1984.

Baines, K. et al., Detection of sub-micron radiation from the surface of Venus by Cassini/VIMS, *Icarus* 148, 307-311, 2000.

Crisp D. et al., Ground-based near-infrared observations of the Venus nightside: 1.27 μm O_2 ($\alpha^1\Delta_g$) airglow from the upper atmosphere, *J. Geophys. Res.* 101, nE2, pp. 4577-4593, 1996.

Galileo images of Venus in UV.

Krasnopolsky, V.A., Venus spectroscopy in the 3000-8000 Å region by Veneras9 and 10, in *Venus-I book*, p.459, 1983.

Meadows, V.S. and D. Crisp, Ground-based near-infrared observations of the Venus nightside: the thermal structure and water abundance near the surface, *J. Geophys. Res.* 101, nE2, pp. 4595-4622, 1996.

Moroz, V.I. et al., Solar and thermal radiation in the Venus atmosphere, *Adv. Space Res.* 5, n11, pp.197-232, 1985.

Stewart et al., Morphology of the Venus ultraviolet night airglow, *J. Geophys. Res.* 85, nA13, pp. 77861-7870, 1980.